

Measurements of fuel and ablator pR in Symmetry-Capsule implosions with the Magnetic Recoil neutron Spectrometer (MRS) on the National Ignition Facility^a

M. Gatu Johnson, J. A. Frenje, C. K. Li, F. H. Séguin, R. D. Petrasso, R. M. Bionta, D. T. Casey, J. A. Caggiano, R. Hatarik, H. Y. Khater, D. B. Sayre, J. P. Knauer, T. C. Sangster, H. W. Herrmann, and J. D. Kilkenny

Citation: *Review of Scientific Instruments* **85**, 11E104 (2014); doi: 10.1063/1.4886418

View online: <http://dx.doi.org/10.1063/1.4886418>

View Table of Contents: <http://scitation.aip.org/content/aip/journal/rsi/85/11?ver=pdfcov>

Published by the [AIP Publishing](#)

Articles you may be interested in

[Forward fitting of experimental data from a NE213 neutron detector installed with the magnetic proton recoil upgraded spectrometer at JETA^a](#)

Rev. Sci. Instrum. **85**, 11E123 (2014); 10.1063/1.4895565

[Neutron spectrometry—An essential tool for diagnosing implosions at the National Ignition Facility \(invited\)^a](#)

Rev. Sci. Instrum. **83**, 10D308 (2012); 10.1063/1.4728095

[Probing high areal-density cryogenic deuterium-tritium implosions using downscattered neutron spectra measured by the magnetic recoil spectrometer^a](#)

Phys. Plasmas **17**, 056311 (2010); 10.1063/1.3304475

[A neutron spectrometer for precise measurements of DT neutrons from 10 to 18 MeV at OMEGA and the National Ignition Facility](#)

Rev. Sci. Instrum. **72**, 854 (2001); 10.1063/1.1323243

[A sensitive neutron spectrometer for the National Ignition Facility](#)

Rev. Sci. Instrum. **72**, 846 (2001); 10.1063/1.1323242



NEW
Model PS-100
Tabletop Cryogenic
Probe Station



*An affordable solution for
a wide range of research*

Measurements of fuel and ablator ρR in Symmetry-Capsule implosions with the Magnetic Recoil neutron Spectrometer (MRS) on the National Ignition Facility^{a)}

M. Gatu Johnson,^{1, b)} J. A. Frenje,¹ C. K. Li,¹ F. H. Séguin,¹ R. D. Petrasso,¹ R. M. Bionta,² D. T. Casey,² J. A. Caggiano,² R. Hatarik,² H. Y. Khater,² D. B. Sayre,² J. P. Knauer,³ T. C. Sangster,³ H. W. Herrmann,⁴ and J. D. Kilkenny⁵

¹Plasma Science and Fusion Center, Massachusetts Institute of Technology, Cambridge, Massachusetts 02139, USA

²Lawrence Livermore National Laboratory, Livermore, California 94550, USA

³Laboratory for Laser Energetics, University of Rochester, Rochester, New York 14623, USA

⁴Los Alamos National Laboratory, Los Alamos, New Mexico 87545, USA

⁵General Atomics, San Diego, California 92186, USA

(Presented 3 June 2014; received 31 May 2014; accepted 18 June 2014; published online 11 July 2014)

The Magnetic Recoil neutron Spectrometer (MRS) on the National Ignition Facility (NIF) measures the neutron spectrum in the energy range of 4–20 MeV. This paper describes MRS measurements of DT-fuel and CH-ablator ρR in DT gas-filled symmetry-capsule implosions at the NIF. DT-fuel ρR 's of 80–140 mg/cm² and CH-ablator ρR 's of 400–680 mg/cm² are inferred from MRS data. The measurements were facilitated by an improved correction of neutron-induced background in the low-energy part of the MRS spectrum. This work demonstrates the accurate utilization of the complete MRS-measured neutron spectrum for diagnosing NIF DT implosions. © 2014 AIP Publishing LLC. [<http://dx.doi.org/10.1063/1.4886418>]

I. INTRODUCTION

The Magnetic Recoil neutron Spectrometer (MRS) on the National Ignition Facility (NIF) was designed to measure the neutron spectrum from Inertial Confinement Fusion (ICF) in the energy range of 4–20 MeV.^{1–5} This energy range covers the essential details in the spectrum. The primary neutron yield (Y_{DT}) is determined by integrating the spectrum from 13 to 15 MeV, and the ion temperature (T_{ion}) is determined from the width of the primary peak. An areal density (ρR) is inferred from the ratio of down-scattered neutron yield in the range 10–12 MeV to the primary neutron yield. Signatures of tertiary neutrons from in-flight reactions are visible in the 15–20 MeV range for DT neutron yields approaching 10^{16} . The shape of the neutron spectrum below 10 MeV also contains essential information on the relative importance of fuel and ablator ρR and ρR asymmetries. Full exploitation of the MRS data in this energy range requires detailed understanding of the background in the MRS measurement.

This paper describes how the background in the low-energy part of the MRS spectrum is characterized through measurements and MCNPX (Monte Carlo N-Particle eXtended) neutron-scattering simulations. We show how the complete MRS spectrum can be used to determine DT-fuel and CH-ablator ρR in DT gas-filled Symmetry Capsule (Sym-Cap) implosions with correct treatment of the background. The fidelity in the background determination is established

through a self-consistency check, where results from fits to different regions of the MRS spectrum are compared. To further establish the fidelity of the analysis, the determined DT-fuel and CH-ablator ρR 's are also compared to and cross-validated against the CH-ablator ρR data measured with the Gamma Reaction History (GRH) diagnostic,⁶ and to the expected fuel ρR based on simulations.⁷

II. NEUTRON BACKGROUND

The primary components of the NIF MRS are a deuterated polyethylene foil positioned 26 cm from Target Chamber Center (TCC), in which neutrons elastically scatter to produce recoil deuterons, a 20-cm² magnet aperture at 596 cm from TCC which selects forward-scattered recoil deuterons, an Ne-Fe-B magnet (located behind the aperture) in which recoil deuterons are momentum analyzed, and an array of nine 4.8×6.8 cm² CR-39 track detectors to record the spectrum of the momentum-separated deuterons (Fig. 1(a)), from which the neutron spectrum is inferred. The detector array is encased in polyethylene shielding to reduce the direct and ambient neutron background. Except for the aperture which is open to the chamber vacuum, most of the MRS is also shielded by the steel chamber wall and a 50 cm thick layer of gunite. The combined shielding reduces the background about two orders of magnitude.

CR-39 detectors are insensitive to x-rays, photons, and electromagnetic background, but they are somewhat sensitive to background neutrons interacting with the detector material.⁸ In addition, intrinsic background due to defects in the CR-39 must be considered. Low MRS signal in the

^{a)}Contributed paper, published as part of the Proceedings of the 20th Topical Conference on High-Temperature Plasma Diagnostics, Atlanta, Georgia, USA, June 2014.

^{b)}Author to whom correspondence should be addressed. Electronic mail: gatu@psfc.mit.edu.

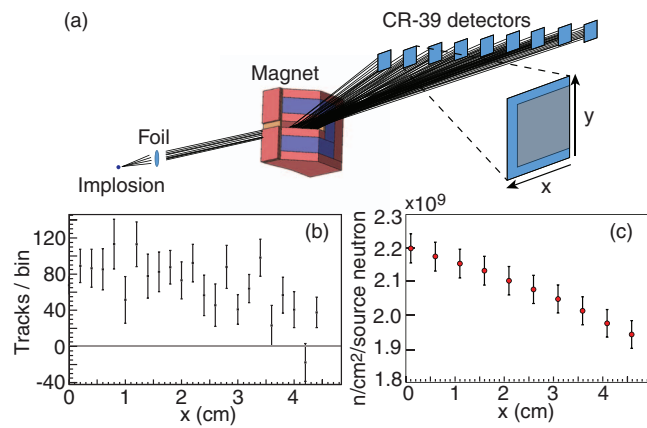


FIG. 1. (a) Schematic drawing of the NIF MRS (not to scale), showing the CD_2 conversion foil, magnet, and nine CR-39 detectors. A zoom-in on detector #2 defines the x (dispersion direction) and y (non-dispersion direction) coordinate system. The central shaded area is the signal region, and the outer blue area is the background region. (b) Background measured by detector #2 as a function of x . The data were obtained from background shot N130628. Note that the measured background varies across the piece. (c) MCNPX-simulated neutron fluence as a function of x -position. As shown, the neutron fluence is predicted to be non-uniform across the piece, with a shape qualitatively similar to the measured background.

presence of high levels of neutron and intrinsic background in the CR-39 data is analyzed using the Coincidence-Counting Technique (CCT).⁹ With this method, the CR-39 is etched and scanned in stages, and only tracks that appear in the same location (within a search-radius of order $50 \mu\text{m}$) in two layers of the plastic separated by $50\text{--}200 \mu\text{m}$ are accepted as signal. Intrinsic background is completely eliminated for layer separation of $100 \mu\text{m}$ or more;⁹ this is the case for all NIF MRS detectors except #1 ($50 \mu\text{m}$) and #2 ($75 \mu\text{m}$). For these detectors, ~ 60 (total) randomly distributed intrinsic coincidences are expected to remain after CCT. CCT also significantly reduces the neutron-induced background. The level of reduction depends on energy and angle of incidence of the background neutrons as well as on layer separation. Two orders of magnitude reduction has been previously observed.⁹ In addition, the number of background neutrons picked up by CCT scales linearly with yield. In contrast, signal deuterons are retained in the analysis as they traverse the CR-39 in straight trajectories practically perpendicular to the two layers.

Each piece of CR-39 is divided into a signal region reachable by the signal deuterons and a background region where no signal is expected (the different regions for CR-39 detector #2 are shown in Fig. 1(a)). After having applied the CCT to the data, the remaining average number of coincidences per cm^2 in the background region is characterized and used to correct for the background across the signal region. Using this type of correction, however, does not eliminate all background as the background does vary across the piece of CR-39. To allow for accurate correction for neutron-induced background, the background was experimentally established on a NULL shot (N130628, $Y_{\text{DT}} = 1.6 \times 10^{15}$) where MRS was fielded without a conversion foil. The background correction as determined on N130628 is now routinely applied to the MRS spectrum. From the measurement, it was found

that the background was distinctly non-uniform across CR-39 detectors #1–5. Fig. 1(b) shows the measured background distribution along x for CR-39 detector #2.

To understand this observation, a detailed MCNPX¹⁰ model of the NIF target bay including the MRS housing and shielding was used to assess the expected distribution of neutron-induced background across the individual CR-39 detectors. The result for CR-39 detector #2 is shown in Fig. 1(c). The simulations show a variation in neutron fluence along the x -direction that is in qualitative agreement with the observation. The level of variation depends on what neutron energy range is considered in the simulation. For all neutrons, the variation is $\sim 13\%$ (see Fig. 1(c)), for neutrons with energy above 2.4 MeV , $\sim 21\%$, and for neutrons with energy above 10 MeV , $\sim 34\%$. To allow for a comparison of simulated and measured results, the processes by which neutrons interact with CR-39 must be considered. For neutron energies below $\sim 10 \text{ MeV}$, elastic n,p scattering is the dominant interaction process. Neutrons below 2.4 MeV are not expected to contribute in CCT for detector #2 because recoil protons with energy less than 2.4 MeV are effectively ranged out in the $75 \mu\text{m}$ of CR-39 between layers. Neutrons above $\sim 10 \text{ MeV}$ are expected to also generate reactions, the signature of which may be different in CCT than elastic n,p reactions. The MCNPX modeling also indicates that the background variation is larger for CR-39 detectors closer to the MRS aperture. The most likely explanation for this result is that the variation of the neutron-fluence background, due to scatter on the inside of the MRS shielding, is larger for the low-energy detectors than for the high-energy detectors (due to larger solid-angle variation).

III. RESULTS FROM SYMCAP EXPERIMENTS

Having a detailed understanding of the characteristics of the background at the different detectors, an accurate determination of the low-energy part of the MRS spectrum can now be made to look at the detailed shape of this part of the spectrum. This was done in a series of five DT-gas filled SymCap implosions,^{11,12} which are indirectly driven implosions with a thick CH-plastic payload to emulate the DT ice in a cryogenically layered implosion. Due to the significantly higher CH ρR than the DT fuel ρR in these implosions, the number of downscattered neutrons from CH becomes comparable to the number of downscattered neutrons from the DT fuel, making this type of implosion an ideal candidate for attempting to separate CH-ablator and DT-fuel ρR contributions to the neutron spectrum. Because of lower convergence, these implosions are also expected to be less affected by low-mode ρR asymmetries than cryogenically layered DT implosions. In this analysis, we neglect any potential low-mode ρR asymmetries (though it should be noted that for two of the shots, N130625 and N130814, an intentional 8% up-down-asymmetry in the laser drive was imposed to seed implosion asymmetry).

Fig. 2(a) shows the reduced MRS spectrum for shot N130625 ($Y_{\text{DT}} = 7.0 \times 10^{14}$). A modeled neutron spectrum (Fig. 2(b)), with a primary-neutron (Gaussian¹³) component, CH- and DT downscattered neutron components, and

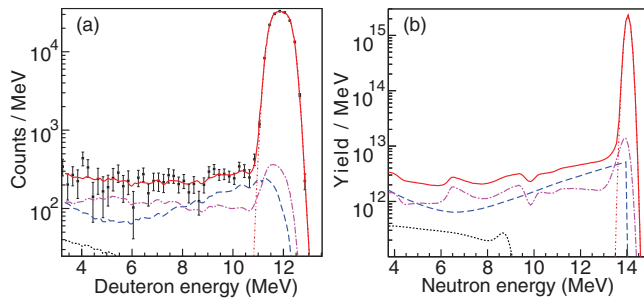


FIG. 2. (a) Reduced MRS spectrum for shot N130625 (black points). (b) Modeled neutron spectrum that provides the best fit to the measured spectrum. A forward fit method is used to determine the magnitude of the DT-fuel (dashed blue) and CH-ablator (long-broken magenta) components in the spectrum, from which the DT-fuel and CH-ablator ρR 's are determined. Primary yield and T_{ion} are determined from the primary DT neutron peak (short-broken red). The solid red curve is the total fit to the measured spectrum. The TT neutron component (dotted black), fixed relative to the DT yield, is also shown to illustrate its insignificance.

a TT-neutron component, is folded with the MRS response function and adjusted until a best-fit to the measured spectrum is found. On the basis of the TT and DT reactivities, the magnitude of the TT component is fixed relative to the DT yield (the TT spectral shape is fixed in this analysis according to the work in Ref. 14.) (The validity of this approach is confirmed by the $Y_{\text{DD}}/Y_{\text{DT}}$ ratios measured on the five SymCaps studied, which are in agreement with the values expected based on reactivities.) The DT-fuel component used to give DT fuel ρR was calculated on the basis of n, D , $D(n, 2n)$,¹⁵ n, T ,¹⁶ and $T(n, 2n)$ cross-sections, scaled

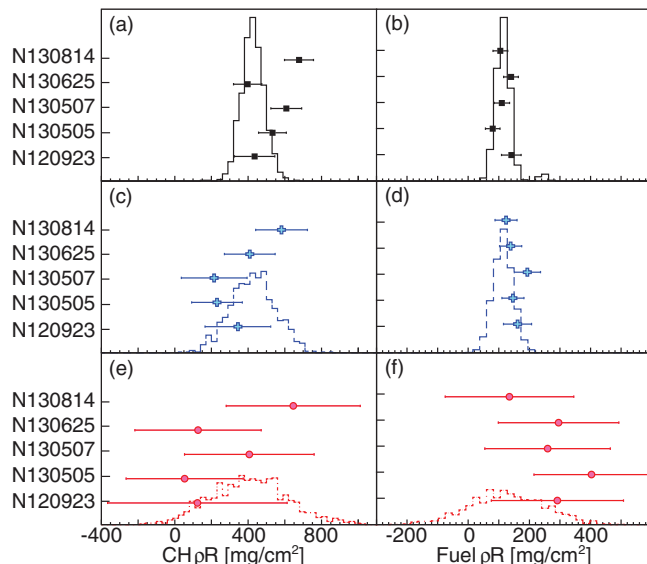


FIG. 3. (a), (c), and (e) CH-ablator ρR and (b), (d), and (f) DT-fuel ρR determined from MRS spectra obtained on five DT gas-filled SymCap implosions. Values are determined from fits to the full spectrum (black points; (a) and (b)), to the $E_d = 7\text{--}11$ MeV range (blue crosses; (c) and (d)), and to the $E_d = 3.5\text{--}7$ MeV range (red circles; (e) and (f)). Also shown are histograms of CH-ablator and DT-fuel ρR 's determined from 1000 fits to synthetic MRS data with seeded $\rho R_{\text{DT}} = 115$ mg/cm² and $\rho R_{\text{CH}} = 440$ mg/cm². The black histograms (a) and (b) were determined from fits to the full spectrum, the dashed blue histograms (c) and (d) from the $E_d = 7\text{--}11$ MeV range, and the dashed red histograms (e) and (f) from the $E_d = 3.5\text{--}7$ MeV range.

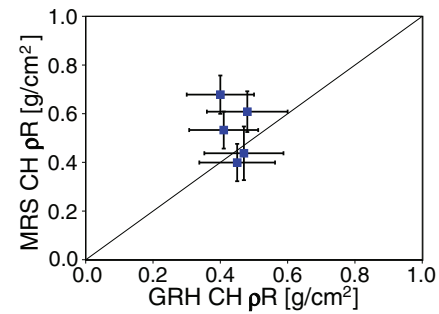


FIG. 4. Comparison of CH-ablator ρR inferred from the GRH and MRS analysis.

for simulated emission profile effects, and the CH-ablator component used to give CH-ablator ρR was calculated using MCNPX for an implosion with 440 mg/cm² CH-ablator ρR , $T_{\text{ion}} = 2.9$ keV, and SymCap-like geometry, to account for multi-scatter and profile effects. From the spectrum shown in Fig. 2(a), a DT-fuel ρR of 140 ± 24 mg/cm² and a CH-ablator ρR of 399 ± 77 mg/cm² were determined. The best fit is describing the spectrum well ($\chi^2_{\text{red}} = 1.1$).

CH-ablator and DT-fuel ρR values determined from the MRS spectrum for the five shots studied are shown in Fig. 3. To confirm the validity of the background correction, fits to the full MRS spectrum were compared to fits constrained to either the low ($E_d = 3.5\text{--}7$ MeV) or high ($E_d = 7\text{--}11$ MeV) energy part of the spectrum. As can be seen from Fig. 2, there are limited features to distinguish the two components in these narrower parts of the spectrum (in particular in the range $E_d = 3.5\text{--}7$ MeV). This is why the error bars from the fits to the narrow part of the spectrum are larger than the error associated with the fit to the total spectrum. These results were also compared to fits to synthetic data (full spectrum fits as well as fits limited to the $E_d = 7\text{--}11$ MeV and $E_d = 3.5\text{--}7$ MeV ranges). Synthetic data were generated by folding a model neutron spectrum such as in Fig. 2(b), with seeded $Y_{\text{DT}} = 8 \times 10^{14}$, $T_{\text{ion}} = 2.7$ keV, $\rho R_{\text{DT}} = 115$ mg/cm² (average MRS result from the five shots), and $\rho R_{\text{CH}} = 440$ mg/cm² (average GRH result from the five shots), through the MRS response function, and then imposing a random Poisson fluctuation around the value in each bin. The results from the fits to the different parts of the spectrum correspond well to the spread in values inferred from fits to the synthetic data. Given the uncertainties involved, the fits from the three parts of the spectrum are in good agreement. The shot-by-shot comparison of MRS and GRH-inferred CH-ablator ρR 's for these shots is shown in Fig. 4. Within error bars, the overall agreement is good, cross-validating results from both diagnostics. The MRS-inferred fuel ρR 's are also in good agreement with expectations based on simulations.

IV. CONCLUSIONS

We report on MRS measurements of CH-ablator and DT-fuel ρR from DT gas-filled SymCap implosions at the NIF. DT fuel and CH ablator ρR 's in the range of 80–140 mg/cm² and 400–680 mg/cm² are obtained, respectively. The

analysis is facilitated by an improved background determination in the low-energy part of the MRS spectrum ($E_n < 10$ MeV). To confirm the validity of the background correction, results from fits to the $E_d = 3.5\text{--}7$ MeV and the $E_d = 7\text{--}11$ MeV spectral ranges are compared to results from fits to the full spectrum. The good agreement between the CH-ablator ρR values derived from MRS spectra and those based on GRH measurements as well as the equally good agreement between the MRS-derived DT-fuel ρR values and those based on calculations establishes the fidelity of the MRS (and GRH) results. This work demonstrates the accurate utilization of the complete MRS-measured neutron spectrum for diagnosing both SymCap and layered implosions at the NIF.

ACKNOWLEDGMENTS

This work was performed under the auspices of the U.S. DOE by MIT under Contract No. DE-NA0001857 and

Lawrence Livermore National Laboratory under Contract No. DE-AC52-07NA27344.

- ¹J. A. Frenje *et al.*, *Rev. Sci. Instrum.* **72**, 854 (2001).
- ²J. A. Frenje *et al.*, *Rev. Sci. Instrum.* **79**, 10E502 (2008).
- ³J. A. Frenje *et al.*, *Phys. Plasmas* **17**, 056311 (2010).
- ⁴D. T. Casey *et al.*, *Rev. Sci. Instrum.* **84**, 043506 (2013).
- ⁵M. Gatu Johnson *et al.*, *Rev. Sci. Instrum.* **83**, 10D308 (2012).
- ⁶D. B. Sayre *et al.*, *Rev. Sci. Instrum.* **83**, 10D905 (2012).
- ⁷S. Weber, private communication (2013).
- ⁸J. A. Frenje *et al.*, *Rev. Sci. Instrum.* **73**, 2597 (2002).
- ⁹D. T. Casey *et al.*, *Rev. Sci. Instrum.* **82**, 073502 (2011).
- ¹⁰MCNPX User's Manual, Version 2.7.0, LA-CP-11-00438, April 2011, see <https://mcnpx.lanl.gov>.
- ¹¹J. D. Kilkenny *et al.*, "Understanding the stagnation and burn of implosions on NIF," *J. Phys. Conf. Ser.* (to be published).
- ¹²S. V. Weber *et al.*, "Simulations of indirectly driven gas-filled capsules at the National Ignition Facility," *Phys. Plasmas* (submitted).
- ¹³L. Ballabio, J. Källne, and G. Gorini, *Nucl. Fusion* **38**, 1723 (1998).
- ¹⁴D. B. Sayre *et al.*, *Phys. Rev. Lett.* **111**, 052501 (2013).
- ¹⁵A. Deltuva, private communication (2013).
- ¹⁶J. A. Frenje *et al.*, *Phys. Rev. Lett.* **107**, 122502 (2011).